Hydrol. Earth Syst. Sci. Discuss., 5, 3557–3604, 2008
www.hydrol-earth-syst-sci-discuss.net/5/3557/2008/

Hydrology and Earth System Sciences Discussions

Papers published in *Hydrology and Earth System Sciences Discussions* are under open-access review for the journal *Hydrology and Earth System Sciences*

Temporal variation of soil moisture over the Wuding River Basin assessed with an eco-hydrological model, in-situ observations and remote sensing

S. Liu[1], X. Mo[2], W. Zhao[3], V. Naeimi[4], D. Dai[3], C. Shu[1], and L. Mao[5]

[1]Key Laboratory of Water Cycle and Related Land Surface Processes, Institute of Geographic Sciences and Natural Resources Research (IGSNRR), Chinese Academy of Sciences (CAS), Beijing, 100 101, China
[2]Key Laboratory of Ecological Network Observation and Modeling, IGSNRR, CAS, China
[3]The Bureau of Hydrology, Yellow River Conservancy Committee, Zhengzhou, 450 004, China
[4]Inst. of Photogrammetry and Remote Sensing, Vienna Univ. of Technology, Vienna, Austria
[5]China Meteorology Administration, National Meteorological Center, Beijing, 100 081, China

Received: 7 October 2008 – Accepted: 7 October 2008 – Published: 6 December 2008

Correspondence to: S. Liu (liusx@igsnrr.ac.cn)

Published by Copernicus Publications on behalf of the European Geosciences Union.

Abstract

For integrative management of soil and water in the Wuding River basin, Loess plateau, China, where severe soil erosion damages are incurred, the ecohydrological behavior of the region is needed to be explored. In this study we focus on the evolution of soil moisture (SM) in the basin. Since there are only twelve years in-situ SM measurements available at two stations from 1992 to 2004, an eco-hydrological processes-based model (VIP, Vegetation Interface Processes model) is employed to simulate the long-term SM, evapotranspiration (E_T), vegetation cover and production variation from 1956 to 2004, for the mechanical analysis of SM change. In-situ SM observations and a remotely sensed SM dataset retrieved by the Vienna University of Technology are used to validate the model. The results show that the model is able to capture seasonal SM variations. The seasonal pattern, multi-year variation, standard deviation and CV (coefficient of the variation) of SM at the daily, monthly and annual scale are well explained by the climatic and ecological factors such as precipitation, temperature, net radiation, evapotranspiration, and Leaf Area Index (LAI, denoted as L_{AI}). The annual and inter-annual variability of SM is the lowest comparing with that for other 11-ecohydrological variables. The trend analysis shows that SM is in decreasing tendency at α=0.01 level of significance. Its significance is lower than that of runoff and that of temperature (α=0.001), whereas higher than that of precipitation (α=0.1). The products of these long-term SM data aim to help integrative management of soil and water resources.

1 Introduction

Soil moisture (SM) at large spatial scale has been becoming a hot topic in hydrology and climatology since last decade. Of the studies, the trend of SM has been paid special attention for its important role in the areas of drought and flood prediction, water resources management, and agricultural production. Besides, the trend analysis

HESSD

5, 3557–3604, 2008

of SM, being related with both water and soil, is an indictor of the effect of land use cover change on hydrological processes.

There are three prevailing methods to do the trend analysis. The first is to draw the linearly regressive trend line over the time series of data to see if it is in upward (increasing) or downward trend (Robock et al., 2000). The second is using the non-parametric Mann-Kendall trend test (Mann, 1945; Kendall, 1975; Hirsch and Slack, 1984) and judging the trend by the trend coefficients (e.g. Sheffield Wood, 2008). The last not the least is to compare the SM averaged at decade, which is broadly used in the related studies in China (e.g. Yan et al., 1999).

It is well recognized that longer-term data series will be better for trend analysis. Unfortunately, all over the world long term SM data are available only at few sites. Hence, the models and remote sensing technique are used to extend the SM data both in space and time.

Remote sensing data can effectively be used to retrieve SM information at regional and global scale, which is an irreplaceable help in the SM study. However, temporal extend of the available remotely sensed SM data is not enough for climate studies yet.

SM is an important element in hydrological cycle closely related to water and energy transfer between soil, vegetation, and atmosphere. Physically based models are used to obtain reliable prediction of SM. So far several SM datasets have been produced using different land surface process models. However most of the models have simple SM schemes (e.g. Liu et al., 2003) or are forced with monthly average, which made the simulated SM results not agree well with the observations (Chen et al., 1997; Entin et al., 1999; Schlosser et al., 2000). It has been shown that much of the global warming so far was at night (Karl et al., 1991, 1993; Folland et al., 1992; Stenchikov and Robock, 1995; Robock et al., 2000). So at least models with diurnal cycle are needed to correctly simulate SM. The SM is also characterized by strong autocorrelation in time, which means that lagged effects in inputs or losses can be as important as those occurring at the time that the impacts are actually observed (Hamlet et al., 2007). A physically-based model with detail soil-vegetation-atmosphere water and energy trans-

fer is needed to correctly simulate long term SM for trend analysis of SM.

Within the long-term trends, there are noticeable interannual and decadal variations in SM for most regions, which weaken the robustness of the trends (Sheffield and Wood, 2008). Hence the interannual and decade variations should be considered while studying the trend of SM.

In this paper, a distributed physically based hydrological model – Vegetation Interface Processes (VIP) model – (Mo and Liu, 2001; Mo et al., 2004a, b, 2005), describing detailed water and energy transfer in soil-vegetation-atmosphere system, is used to explore the trend of SM in a large scale basin, Wuding River Basin, in Loess Plateau. Observed data by both in-situ and remotely sensed SM data from 1992 to 2004 are used to validate the model. The validated model is used to obtain the long term SM series. The Mann-Kendall scheme is then used to identify the SM trend. The results of the work aim to help integrative management of soil and water resources.

In the following section the methodology is introduced briefly. The study region and datasets are described in Sect. 3. The results of the analysis are given in Sect. 4, and the discussions are in Sect. 5. Finally, a short conclusion is made in Sect. 6.

2 Method

2.1 Model introduction

VIP model is used to simulate hydrological cycling over the Wuding River basin. Its ecological and hydrological processes are implemented by coupling a one-dimensional soil-vegetation-atmosphere transfer (SVAT) scheme, a distributed runoff routing scheme (kinematic wave) and a vegetation dynamic scheme. The digital elevation model (DEM) is employed to create the channel flow directions corrected with the realistic river pattern. Geographical information of vegetation type and land use is incorporated to assign the land surface attributes spatially (Mo and Liu, 2001; Mo et al., 2004a, b, 2005). Here estimation of ET, SM and runoff are briefly introduced.

Energy fluxes are described with a two-source scheme discerning canopy and soil surface separately (Shuttleworth and Wallace, 1985). The total canopy E_T ($\mathrm{kg\,m^{-2}\,s^{-1}}$) composed of soil evaporation, canopy transpiration and its intercept evaporation is expressed respectively in the form similar to Penman-Monteith equation (Monteith and Unsworth, 1990). The SM budget is estimated with a six-layer scheme. The depth of soil layer is 2.0 m. Soil hydraulic parameters are estimated with the Clapp and Hornberger (1978) empirical formula.

The magnitude and timing of overland runoff are affected by many factors, such as rainfall intensity, SM condition and land use. The overland runoff is treated as the ratio of the square of the precipitation, deducted the canopy interception, to the summation of this precipitation and the SM deficit in the root zone (Choudhury and Digirolamo, 1998).

2.2 Trend analysis method

Mann-Kendall test (Gilbert, 1987) for trend and Sen's slope estimates (by using Excel template MAKESENS, developed by Salmi et al., 2002) is used for detecting and estimating trends in the time series of annual mean of SM. The Mann-Kendall test for a monotonic trend testing in the data and the Sen's method for estimating slope of the trend are introduced as follows, respectively.

Assuming the data values x_i of the time series can be assumed to obey the model

$$x_i = f(t) + \varepsilon_i \quad (1)$$

where $f(t)$ is a continuous monotonic increasing or decreasing function of time and the residuals ε_i is assumed to be from the same distribution with zero mean.

To test the null hypothesis of no trend, H_0, i.e. the observations x_i are randomly ordered in time, against the alternative hypothesis, H_1, where there is an increasing or

decreasing monotonic trend, a statistic is constructed as follows

$$S=\sum_{k=1}^{n-1}\sum_{j=k+1}^{n}\mathrm{sgn}(x_j-x_k) \tag{2}$$

where x_j and x_k are the annual values in year j and k, $j>k$, respectively, and

$$\mathrm{sgn}(x_j-x_k)=\begin{cases}1, & \text{if } x_j-x_k>0\\ 0, & \text{if } x_j-x_k=0\\ -1, & \text{if } x_j-x_k<0\end{cases} \tag{3}$$

The number of annual values in the studied data series is denoted by n.

The expectance value of the statistic S is zero, and the variance of S is

$$\mathrm{Var}(S)=\frac{1}{18}\left[n(n-1)(2n+5)-\sum_{p=1}^{q}t_p(t_p-1)(2t_p+5)\right] \tag{4}$$

where q is the number of tied groups and t_p is the number of data values in the pth group.

By using the statistic S and the above variance VAR(S), a new statistic Z is constructed to be used in the test for n being larger than 10, i.e.

$$Z=\begin{cases}\frac{S-1}{\sqrt{\mathrm{VAR}S)}} & \text{if } S>0\\ 0 & \text{if } S=0\\ \frac{S+1}{\sqrt{\mathrm{VAR}S)}} & \text{if } S<0\end{cases} \tag{5}$$

A positive (negative) value of Z indicates an upward (downward) trend. The statistic Z has a normal distribution. In this case, $Z_{1-\alpha/2}$ is obtained from the standard normal cumulative distribution tables. As shown in Fig. 1, if the absolute value of Z equals or exceeds the specific value $Z_{\alpha/2}$, it means that in this case at the significant level of α, the probability of accepting H_0 is very rare, in another words, the existence of a

monotonic trend (H_1) is very probable. For the significance level of α=0.01 as shown in Fig. 1, it means that there is a 1% probability that the values x_i are from the normal distribution and with that probability we make a mistake when rejecting H_0 of no trend.

For an existing trend (as change per year), $f(t)$ in Eq. (1) is equal to:

$$f(t)=\mu t+B \tag{6}$$

where μ is the slope and B is a constant.

To get the slope estimate of μ, the slopes of all data value pairs are at first calculated as:

$$\mu_i=\frac{x_j-x_k}{j-k} \tag{7}$$

where $j>k$. If there are n values of x_j in the time series we get as many as $N=C_n^2=n(n-1)/2$ slope estimates μ_i.

In Sen's method (cited by Salmi et al., 2002), the slope estimate μ is the median of all the values of μ_i (i=1, 2,. . . , N). All the values of μ_i are ranked from the least to the top and the Sen's estimator is

$$\mu=\mu_{[(N+1)/2]}, \text{ if } N \text{ is odd} \quad \text{or} \quad \mu=\frac{1}{2}\left(\mu_{[N/2]}+\mu_{[(N+1)/2]}\right), \text{ if } N \text{ is even} \tag{8}$$

In order to give a two-sided confidence interval about the slope estimate, at first a working variable is defined as

$$C_\alpha=Z_{1-\alpha/2}\sqrt{\mathrm{VAR}(S)} \tag{9}$$

Next, $M_1=(N-C_\alpha)/2$ and $M_2=(N+C_\alpha)/2$ are computed. Thus, the lower and upper limits of the confidence interval, $\mu_{\min}$ and $\mu_{\max}$ are defined as the M_1^{th} largest and the $(M_2+1)^{\text{th}}$ largest of all these ordered slope estimates of μ_i. If M_1 is not a whole number, the lower limit is interpolated. Correspondingly, if M_2 is not a whole number, the lower limit is interpolated.

With the slope estimate μ, it is easy to obtain the estimate of B from Eq. (6) as $x_i - \mu t_i$. The median of these values gives an estimate of B. The estimates for the constant B for the confidence interval are calculated by a similar procedure of μ.

In the following trend analysis, the confidence intervals at two different confidence levels α=0.01 and α=0.05, i.e. the lines of the 99% and 95% confidence intervals are calculated.

3 Materials

3.1 Basin description

The Wuding River basin (108°18′~110°45′ E, 37°14′~39°15′ N) with an area of 30 260 km^2 is located in a transition zone from farmland and grassland to desert over the Loess Plateau (Fig. 2). Elevation in the basin ranges from 600 m to 1800 m. The northwestern part of the region is composed of sand desert with a gentle undulation landscape and the southern part is characterized as steep hill-slopes with incised channels. The soil texture is principally categorized as sandy loam, sandy silt, sand, silt and coarse sand in the basin. Since the basin locates in a temperate and semi-arid monsoon climate zone, the annual mean air temperature ranges from 7.9°C to 11.2°C and the annual precipitation from 300 mm to 550 mm decreasing gradually from the southeastern to northwestern part. Precipitation events mainly occur in summer monsoon season (June to September) along with occasional heavy storms. The average annual runoff depth over the past thirty years is about 35 mm.

3.2 Data

The data used in study can be categorized as: (1) in-situ and remotely sensed SM data, (2) meteorological and other hydrological data, and (3) land surface characteristic data that are described briefly as follows.

3.2.1 SM data

In-situ data at two SM measurement sites, Suide (110.21° E, 37.5° N) and Yulin (109.7° E, 38.23° N), are available in the Wuding River Basin. The locations of stations are indicated by cross symbols in Fig. 2. SM measurements in these sites were made with gravimetric method from the top layer down to the 50 cm at the 10 cm interval on the 8th, 18th and 28th each month from 1992 to 2005 ($g\,g^{-1}$). The in-situ SM data were used to validate the model.

In addition to in-situ SM measurements, a global remotely sensed SM dataset is employed to validate the model at regional scale, which is retrieved from long term scatterometer measurements using a change detection method developed in the Vienna University of Technology (TUW) (Wagner et al., 1999). In the TUW retrieval algorithm, SM time series are extracted from backscatter measurements of the scatterometers onboard the European Remote Sensing satellites ERS-1 and ERS-2. Due to the penetration depth of scatterometer signal decreasing with increasing soil moisture, the TUW data represent the water content in 2–5 cm soil depth in relative units between the driest and wettest conditions in the period of 1 August 1991 to 31 May 2007 (data acquisition has been done irregularly with on average two measurements per week), resampled into a 12.5×12.5 km equally-spaced discrete global grid, which is indicated by solid dots in Fig. 2.

3.2.2 Meteorological and other hydrological data from 1956 to 2004

The climatic data at 15 stations in and around the basin from 1956 to 2004 are used to drive the model. The atmospheric forcing is daily maximum and minimum air temperature, humidity, wind speed, precipitation and sunshine duration. The daily climatic data were interpolated to the whole basin with the inverse distance square method. Discharge data from 1956 to 2004 were used for model validation.

3.2.3 Land surface characterization data

The model characterizes the land surface as topography, vegetation type/density, soil texture and land use. Digital elevation model was obtained from the topographic contour map at 1:250 000 scale, which can be created as fine as 150 m resolution terrain raster. Leaf Area Index (LAI, denoted as L_{AI}) mainly features the vegetation density, which was estimated by the VIP model. Soil texture data were retrieved from the map at the scale of 1:14 000 000 (Institute of Soil Science, Chinese Academy of Sciences, 1986). Land use data at the scale of 1:100 000 (http://www.resdc.cn/) in 1980s was used. The land-use/cover was classified into six types, namely, farmland, mixed forest, dwarf shrub, grassland and desert with fractions of 29%, 3%, 4%, 43% and 21%, respectively. Farmland is mainly located in the stream valleys, slopes and terraces in the southern part, on which crops, such as maize, millet, soybean and rice, are planted. Natural vegetation cover in the basin is generally sparse. Excess reclamation and over-grazing have induced vegetation degradation, soil erosion and desertification, which are the main causes of environmental vulnerability in this basin.

3.2.4 Model implementation and analysis

Water and energy balance components were calculated for each grid separately, neglecting flux exchanges between grids. Because irrigated field only occupies a small amount of farm land, the farm land is assumed as fully rain-fed land. Since the energy fluxes response to the atmospheric driving forces much more quickly than those to hydrological processes in the soil, the energy budget module was run on hourly and soil water module was on daily step, respectively.

Geographical and vegetation cover data all were sampled respectively into the same resolutions of 8 km. The use of 8 km originally is used to match with the resolution of global NDVI data from NOAA in our other research work.

HESSD
5, 3557–3604, 2008

The data time period is from 1956–2004. The model was validated over the period of 1991–2004, by using the ten-day in-situ SM data at the two points, and the two measurements per week's remote sensed SM data grid by grid over the basin.

The SM data simulated by the model represent the relative water contents of soil surface (2.5 cm, wc/wcsat). As the TUW scatterometer soil moisture data are defined as normalized relative water content, the values of which range between 0 and 100%, both the modeled and in-situ data are scaled with TUW scatterometer data to have uniform datasets by using the following formulation for the validation.

$$
\begin{aligned}
&\mathrm{Range}^{\mathrm{VIP}} = \max(\mathrm{SM}^{\mathrm{VIP}}) - \min(\mathrm{SM}^{\mathrm{VIP}}) \\
&\mathrm{Range}^{\mathrm{obs}} = \max(\mathrm{SM}^{\mathrm{obs}}) - \min(\mathrm{SM}^{\mathrm{obs}}) \\
&\mathrm{Range}^{\mathrm{TUW}} = \max(\mathrm{SM}^{\mathrm{TUW}}) - \min(\mathrm{SM}^{\mathrm{TUW}}) \\
&\mathrm{SM}_i^{\mathrm{VIP\_normalized}} = (\mathrm{SM}_i^{\mathrm{VIP}} - \min(\mathrm{SM}^{\mathrm{VIP}})) \times \mathrm{Range}^{\mathrm{TUW}} / \mathrm{Range}^{\mathrm{VIP}} + \min(\mathrm{SM}^{\mathrm{TUW}}) \\
&\mathrm{SM}_i^{\mathrm{obs\_normalized}} = (\mathrm{SM}_i^{\mathrm{obs}} - \min(\mathrm{SM}^{\mathrm{obs}})) \times \mathrm{Range}^{\mathrm{TUW}} / \mathrm{Range}^{\mathrm{obs}} + \min(\mathrm{SM}^{\mathrm{TUW}})
\end{aligned}
\tag{10}
$$

For the comparison at the regional scale, we first output the latitude and longitude of the point of TUW data falling with the basin. Then we output the VIP SM data at those 8-km spacing grids with the latitude and longitude matching with those of TUW. These VIP SM data are used to compare with the TUW data.

By using the validated model, the SM was simulated from 1956 to 1991 at the grid of 8 km. One simulation year of 1956 were repeated as spinning-up. With these long-term SM data averaged over the whole of the basin, the trends were detected with M-K method and Sen's method. The seasonal patterns of various hydro-climate elements are compared with each other. Coefficient of variation (Liu et al., 2001), denoted as C_v, is used to further analyze the temporal characteristics of SM variation.

4 Results

4.1 Validation of the model

Figure 3 shows the simulated SM data at the Suide and Yulin stations compared with the in-situ SM observations and the TUW scatterometer-derived SM data. The correlation coefficients (and Nash-Sutcliffe coefficient) between the simulation and the in-situ data are 0.58 (43%) and 0.52 (−106%) at Suide and Yulin, respectively. The correlation coefficients (and Nash-Sutcliffe coefficient) between the simulation and the TUW data are slightly higher, being 0.65 (38.5%) and 0.66 (40.8%) at Suide and Yulin, respectively. Although the Nash-Sutcliffe coefficient are not high in all the cases, the simulated SM data by VIP model can catch the variation trend and match well with the observed SM at Suide and Yulin. Relatively speaking, TUW SM data are in more closely matched with VIP data. The very low Nash-Sutcliffe coefficient between in-situ observation and the VIP simulation at Yulin may be due to the sparse in-situ observation data when SM is low. It has been argued by previous authors that the utility of the Nash-Sutcliffe efficiency as a performance measure may be limited by bias in its evaluation (Garrick et al., 1978; Ma et al., 1998; Weglarczyk, 1998; Sauquet and Leblois, 2001), especially because the square summation between the observation and the simulation (σ_i^2) is not necessarily smaller than the square summation (σ_{obs}^2) between the observation and the mean of the observation, when σ_{obs}^2 is small. More in detail is shown in Mo et al. (2006a).

In the regional scale, the differences of averaged relative SM (%) over the 6 years (1992–1997) between VIP_SM and TUW_SM are shown in Fig. 4. Generally, at regional scale the averaged simulation matched with averaged TUW data well in most of the season except the obvious biases occurring in winter. In winter the simulated SM is larger than the value of TUW data. It is worthy to mention that this cannot be treated as real large errors as the TUW data in winter should be used in caution. The backscatter

from frozen soil surface behaves like the backscatter from dry soil. Depending on the wetness of snow cover, backscatter signal changes sporadically. It is very difficult to predict the behavior of backscatter from a surface covered with snow (Albergel et al., 2008).

4.2 The seasonal variation and multi-year variability of SM at daily and monthly scales

Before studying the general trend of the SM over the recorded years, it is meaningful to see the variation of SM at various temporal scales including the daily, monthly, annual and decadal scales.

We first look at the seasonal cycle of SM and its multi-year variability (Fig. 5). It is seen that SM follows the summer monsoon pattern in that the maximum SM both for surface and root zone happens in summer, so did for all other influential factors as shown in Figs. 6 and 7a, b. During the spring, over the basin SM is relatively stable. There is a sharp decrease of soil water from February to March (in surface) or from January to February (root zone), because the lowest temperature in the basin is not in December, but in January (Fig. 6). This makes the soil surface or the whole of soil profile frozen, with a little lag over the basin, causing the minimum SM in the earlier spring. The small peak of root-zone SM in May is corresponding to the snowmelt because of warmer weather (higherer temperature in Fig. 6), which makes some frozen water turn to be SM and runoff. This also causes the spring flood in runoff (Q in Fig. 6), but the time is in March, as surface water (river) gets warm earlier than the soil water.

Besides the control by atmospheric forcing factors, plant influences SM too. The SM increases rapidly to 15% in the surface and 12% in the root zone as the growing season progresses (toward maximum plant growth, see L_{AI} in Fig. 7b). It becomes stable as the vegetation completes its growth cycle. It is easy to see that the peak of surface SM is earlier than the peak of L_{AI} and root zone SM, implicating that plant's sole reliability on rainfall for moisture. During the vegetation growth to the maximum L_{AI}, plants water demand is high. Due to concentrated precipitation during this period,

high SM condition is lasting. Since precipitation gets lower in September than that in August, SM thus decreases.

The maximum of E_T happens in August, which is matched with the maximum of net radiation (R_n) and precipitation (P) (Fig. 7a, b). The component of E_T from canopy (E_C) and intercepted water by vegetation (E_I) reaches the maximum in August and September which is corresponding to the high L_{AI} in September due to high water consumption by the vegetation. Although the component of E_T from soil (E_S) also reaches the highest in summer due to high temperature and precipitation, its maximum not happens in September when the leaf covers most. The maximum of E_S reaches maximum in July when there are much water in soil surface for evaporation. The ratio of E_C to E_T is much higher than the ratio of E_S to E_T in the seasons other than winter, which makes the pattern of total E_T being similar to E_C at most. The relationship of the two ratios is opposite in winter, where the values for both E_T and the components are small.

The patterns of C_V can be categorized into two. The first is the C_V pattern essentially matching with the patterns of the variables, such as root Zone SM, Q, L_{AI}, and E_C. The second is the C_V pattern being right opposite to the patterns of the variables, such as surface SM, P, T, R_n, E_T, E_S and E_I. For each pattern, the time for the peak (or trough) appearance of the variable is not necessarily matched with the time for that of the C_v.

Generally, the multi-year variability of SM over the 48 years (1956–2004) is the least comparing with other ecology-climate-hydrological variables (Table 1). Over the years, runoff at the cross-section of the basin has been used as an important index to do trend analysis because of the relative easy data availability (e.g. Zhang et al., 1998; Qian et al., 1999; Xu, 2004; Li et al., 2008). However, strong variation of runoff itself may make it confused to get a trend. Comparing with runoff, SM, with lower multi-year variability, may be a better and important hydrological component to explore the change of hydrological elements in the Wuding River basin. This encourages us using SM to describe the ecological-climatic-hydrological trend in the basin.

It is seen that the multi-year change of the averaged SM over the root soil layer is milder than that of the surface SM (Fig. 5). Over the years, there is a largest variability of SM in the surface at the spring peak and lowest variability at the summer peak. This is matched with the lowest variability of the precipitation peak in summer (Fig. 6). Oppositely, there is a largest variability of SM in the root zone at the summer peak and lowest variability at the spring peak, illustrating that surface SM is closely related with precipitation and net radiation, and SM in root zone is more related with evapotranspiration, influenced more comprehensively by both the atmospheric forcing and vegetation dynamics (Fig. 7).

No matter how high or low the variability of SM in summer is, the seasonal cycles of C_V for surface and root zone SM are obvious, a feature in rainfed situation as in our case. For irrigation case instead, the C_V's variation is much stable (Mahmood and Hubbard, 2004). Under variable hydro-climatic condition (precipitation and temperature), plant demand of moisture and insufficient water supply result in the alternative peak and minimum pattern of SM variability.

By comparing the seasonal cycle and its variability with the monthly (Figs. 5–7) and daily SM (Figs. 8–10), it is seen that the seasonal cycles are similar to both the SM and its influential variables. As expected, changes in SM variability from one to the next month are not as drastic as those at the daily scale. Overall, the monthly variability is relative "smooth" compared to the daily scale, with all the means of the C_V at the monthly scale being less than the means of C_V at the daily scale (Table 1, and Fig. 11). More varying local hydro-climatic conditions at daily scale, namely, wet or dry, are averaged monthly, reducing SM variability at monthly scales. As some variability has been averaged, some patterns are clearer at monthly than at daily scale. For example the double peak of runoff and SM is figured out at the monthly scale, which is hided at the daily scale.

It is worthy to point out that for variability analysis, the value of the variable, its standard deviation and its C_V should be used conjunctively for a more comprehensive analysis. Only using standard deviation or C_V for variability analysis is not enough (Liu et

HESSD
5, 3557–3604, 2008

al., 2001; Mahmood and Hubbard, 2004). For example, the standard deviation of R_n in summer is larger than that in winter season. However, the C_V in summer is the lowest. Usually, the relationship between the standard deviation and the value is positive and the relationship between C_V and the value itself of the variable (and the standard deviation) is negative (Fig. 12). There is a minor shortcoming in using C_V for variability analysis. For example, when the value is turning from negative to positive or vice versa, such as for R_n and T (Figs. 6, 7, 9 and 10), the value of C_V is unexpectively high. When the value is at the turning point from high to low and when the mean values are very low, such as in the L_{AI} and E_C cases, the C_V values are also very high. However, this is not necessarily meaning that the multi-year variability at this time is much larger than that in other periods.

4.3 The interannual variation of SM and its variability within each year

The interannual variation of SM and its within-year variability are shown in Fig. 13. There is a decreasing tendency for SM both in the surface and the root zone. Year 1999 is the driest among the simulation years, which matched with the records showing that there was Wuding flood in 1999 (Xu et al., 2000). The within-year variability keeps the same over the years, also seen in Fig. 14. This pattern follows that of precipitation. So did for runoff. We can see that although the value of SM, P and Q are in decreasing tendency, their within-year variability keeps relatively stable. Comparing with P and Q and all other variables (Figs. 15 and 16 and Table 1), the within-year variability of SM are the least. This again encourages us using SM to explore the change signal of eco-climate-hydrological processes in the basin.

It is clear that over the years, the basin is getting warmer, but the annual variation of temperature is getting smaller, showing that the seasonal cycle of temperature is weakened over the years. This is one of the main factors to cause the L_{AI} increasing, the same conclusion drawn by Mo et al. (2006b) by using NDVI data from NOAA/AVHRR from 1981–2001. Over the years, R_n, E_T and its components remain stable, which shows the compensation effect of precipitation and temperature.

Table 2 shows that the SM is higher than the multi-year average in 1950s, 1960s and 1970s. Since then, it keeps drying in 1980s, 1990s and 2000s. Averagely, root zone SM decreases at the rate of 0.01 cm cm^{-3} per decade, this is in agreement with the trend analysis by Nie et al. (2008) who found the SM at the top 50 cm in this region decreases at the rate of 0.00 072 kg kg^{-1} based on the observed data from 13 stations from 1981 to 1998.

One interesting phenomenon is that the decreasing tendency of precipitation has been shown in 1970s already, so did in runoff with an immediate correspondence. However, the decreasing tendency of SM has a delay, which appears only in late of 1980s. This implies that there is a lag in SM's response to precipitation.

4.4 The total variation trend of SM over the 48 years

The M-K method is used to explore how significant of the trend is. Although there is a suggestion to use the SM in summer (June, July, August) to test the trends of SM as summer drying would accompany global warming (Robock et al., 2005), the mean SM over a year is used in the trend analysis in a more comprehensive way.

Some studies made the variables standardized at first before they did the trend analysis (Zhao and Yan, 2006). Scaling the axes, or standardizing the variables is a common technique (e.g. Liu et al., 2001; Ouarda et al., 2001; Mo and Beven, 2004; Riad et al., 2004). Application of such transformations prior to the analysis attempts to remove the influence of scaling effects from the analysis, with the aim to obtain a simpler expression (Ouarda et al., 2001). Furthermore, when plotting the results for a large number of catchments, variables with the largest means tend to dominate the display. As discussed by Friendly and Kwan (2003), scaling axes can effectively result in an incoherent display in which no systematic trends or relations can be distinct. However as shown in Liu et al. (2008), scaling may also bring the uncertainty of the results. We thuse still use the original SM for trend analysis.

From Table 3, it shows that the Wuding River is in drying tendency at α=0.01 level of significance. Runoff and precipitation are also in decreasing tendency. Temperature

is in increasing tendency. The significance of SM is lower than that of runoff and temperature (α=0.001), but higher than that of precipitation (α=0.1). The tendency of net radiation (R_n), Evapotranspiration (E_T), transpiration (E_C), soil evaporation (E_S), canopy intercept (E_I) is not clear in that the Mann-Kendall test indicates a decreasing trend at the less significance level than α=0.1, and the Sen's slope gives non-negative slope even at the 1% confidence interval.

For comparison, we also did the trend analysis by using standardized data. We found that the results of Test Z and the significance were the same as those by using the original variables as shown in Table 3. The only differences were the values of slope estimate Q and the constant B.

It is interesting to see from Table 3 that although soil is in drying tendency, vegetation productivity (NPP – net primary productivity, especially GPP – gross primary productivity) is in increasing tendency. It is seen that the temperature is in increasing tendency. In North China, it is found (Liu et al., 2008) that if not considering CO_2 fertilization effect, crop yield is reduced with an increase in temperature. However, if considering CO_2 fertilization, crop yield may increase. As our model not only deals with hydrological process, but also with vegetation dynamics, the response of productivity may be affected by the precipitation, CO_2 fertilization and temperature. It is thus understandable that a drier soil may produce higher vegetation productivity.

5 Discussions

5.1 North drying?

The drying tendency in the north of China, *Northern Drying*, has been paid strong attention by many documented studies recently. Tao et al. (2003) produced a long-term SM data over China, represented by soil deficit index, from 1946 to 1995 by using a conceptual model. They found there was a trend toward soil drying in the North China Plain and the Northeast China Plain during this period. By using the observed SM data from 35 stations over North China from 1981 to 2002, Zhao and Yan (2006) found that the whole trends of annual mean SM storage averaged by different soil layers from

soil surface to top 50 cm was decreasing generally. By using SM dataset from direct gravimetric measurements within the top 50-cm soil layers at 178 SM stations in China covering the period of 1981–1998, Nie et al. (2008) found that there are increasing trends of SM for the top 10 cm, but decreasing trends for the top 50 cm of soil layers in most regions.

These studies are from a larger scale, with either shorter-term observed data or long-term data simulated by a simple model scheme. Our study further identifies this *Northern Drying* phenomenon, but with long term (48 years) SM data for Wuding River, a large Basin in Northeast China, simulated by a process-based eco-hydrological model with a detail water cycle evolution at diurnal scale.

The same drying trend was also found in West Africa, as driven by decreasing Sahel precipitation. For most of other areas in the world and in some parts of China, the trends are different. For example in Ukraine, Russia, Mongolia (Robock, 2000; Robock and Li, 2006) and most parts of the US (Robock, 2000; Andreadis and Lettenmaier, 2006; Sheffield and Wood, 2008), soil was found in wetter tendency. In the far North China Qaidam Basin of Qinghai Province in northwestern China, Yin et al. (2008) reconstructed the SM conditions from 566 to 2001 and revealed a general trend toward a wetter condition during the most recent 300 years. Tao et al. (2003) found there was a significant increase in SM levels in Southwest China, and a generally insignificant increase or decrease trend in SM levels in Southeast China. Europe, southeast and southern Asia appears to have not experienced significant changes in SM (Sheffield and Wood, 2008).

5.2 Man-made North drying or nature-made

The catchment of the Wuding River, in the Loess plateau of China, is one of the well-known areas incurred most serious soil and water loss and thus becomes one of the main tributaries to produce sediments for the Yellow River. In order to control the soil and water loss, it has taken many soil water conservation countermeasures in the basin, including planting trees, building terraces and constructing checking dams.

These countermeasures not only mitigate the sediment yield from the basin but also change the hydrological processes in the basin via land use and cover change (LUCC). Therefore any changing tendency from the observed data may be contributed by human activities or climate change. There has been a big challenge to differentiate these two contributions. There are some methods such as "baseline" method (Lorup, 1998; Yang et al., 2005; Li et al., 2008), "regression" (e.g. Xu, 2004) and "optimal fingerprint" method (Hasswlmann, 1997; Allen and Scott, 2003; Zhang et al., 2008) to deal with this problem. In our research the long-term SM data are simulated by actual atmospheric forcing, the trend shown by the data should reflect more the influence of climate.

From the M-K analysis, it is found that runoff and precipitation are in decreasing tendency at higher (α=0.001) and lower (α=0.1) level of significance than the level of significance of SM (α=0.01). Air temperature is in increasing tendency at α=0.001 level of significance. As runoff is the observed data, its tendency may reflect the combination of climate and human activity effects.

The decrease in precipitation seems the primary reason for the trend of SM. Logically, with the increase in temperature in Wuding River, E_T may increase consequently, and will further reduce the soil water storage. However in our case the total evapotranspiration and canopy transpiration shows decreasing trend, at insignificant level though. Soil evaporation shows decreasing trend at the significant level of α=0.05. Actually, ET is not linearly related with temperature as described by VIP, which plays an complicate role in temperature-evapotranspiration-SM relationship. In this semi-arid basin, annual ET is mainly regulated by precipitation.

6 Conclusions

The *Northern Drying* phenomenon is found in the Wuding River, China, one of areas incurring most serious water and soil loss. As the basin just has short-term observed soil moisture (SM) data at two stations, an eco-hydrological processes-based model (VIP, Vegetation Interface Processes model) was used to get the long-term daily SM data from 1956 to 2004 to explore this trend.

HESSD
5, 3557–3604, 2008

The model is at first validated by both the in-situ SM data at the two stations and the remotely sensed SM data produced by the Vienna University of Technology (TUW). The averaged TUW_SM data over 189 points matched with the simulated SM by VIP well except significant differences in winter. Although there are differences between the simulation and measured/remotely sensed SM data, their variation trends are matched each other quite well. From the first aspect, this encouraged us to use the model to simulate the long term SM data from 1956 to 2004 for the trend analysis.

With the longer term SM data, the seasonal cycle, summer monsoon pattern, and multi-year variation are analyzed based on the values of SM themselves, their standard deviation and the coefficients of the variation at the daily, monthly and annual scale. The temporal variation patterns are well explained by the other influential factors such as precipitation, temperature, net radiation, E_T and L_{AI}. This encourages us to use the data for the trend analysis from the second aspect.

It is found that the multi-year and within-year variability of SM is the lowest comparing with that for another 11 ecological-climatic-hydrological variables. This, from the third aspect, encourages us using SM data for the trend analysis. For a variable which has a mild change over years, to identify its trend is more meaningful than to identify the trend for a much varying variable.

The trend analysis is then done by the MAKENSES toolkit based on the long term simulated SM data. It shows that SM is in decreasing tendency at α=0.01 level of significance, confirming the *Northern Drying* phenomenon as shown in the documented studies done elsewhere. Its significance is lower than the significance of the decreasing tendency of runoff and increasing tendency of temperature (α=0.001) and higher than the decreasing tendency of precipitation (α=0.1). This indicates that the change of SM is not only due to the climate (precipitation) but also other factors.

Acknowledgements. Great thanks to Chinese National Natural Sciences Foundation (40671033 and 40671032), China MOST project (2006AA10Z228,2009CB421307), Chinese Meteorological Administration special project (CCSF2007-33) and GLOBESCAT project (Austrian Science Fund).

References

Albergel, C., Rüdiger, C., Carrer, D., Calvet, J.-C., Fritz, N., Naeimi, V., Bartalis, Z., and Hasenauer, S.: An evaluation of ASCAT surface soil moisture products with in-situ observations in southwestern France, Hydrol. Earth Syst. Sci. Discuss., 5, 2221–2250, 2008, http://www.hydrol-earth-syst-sci-discuss.net/5/2221/2008/.

Allen, M. R. and Stott, P. A.: Estimating signal amplitudes in optimal fingerprinting. Part I: Theory, Clim. Dynam., 21, 477–491, 2003.

Andreadis, K. M. and Lettenmaier, D. P.: Trends in 20th century drought over the continental United States, Geophys. Res. Lett., 33, L10403, doi:10.1029/2006GL025711, 2006.

Chen, T. H., Henderson-Sellers, A., Milly, C. D., et al.: Cabauw experimental results from the Project for Intercomparison of Land-surface Parameterization Schemes (PILPS), J. Climate, 10, 1194–1215, 1997.

Choudhury, B. J. and DiGirolamo, N. E.: A biophysical process-based estimate of global land surface evaporation using satellite and ancillary data I. Model description and comparison with observations, J. Hydrol., 205, 164–185, 1998.

Clapp, R. B. and Hornberger, G. M.: Empirical equations for some soil hydraulic properties, Water Resour. Res., 14, 601–604, 1978.

Entin, J. K, Robock, A., Vinnikov, K. Y., Zabelin, V., Liu, S., Namkhai, A. and Adyasuren, T.: Evaluation of Global Soil Wetness Project soil moisture simulations, J. Meteorol. Soc. Jpn., 77, 183–198, 1999.

Folland, C. K., Karl, T. R., Nicholls, N., Nyenzi, B. S., Parker, D. E., and Vinnikov, K. Y.: Observed climate variability and change. Climate Change 1992, The Supplementary Report to the IPCC Scientific Assessment, edited by: Houghton, J. T., Callander, B. A., and Varney, S. K., Cambridge University Press, 135–170. 1992.

Friendly, M. and Kwan, E.: Effect ordering for data displays, Comput. Stat. Data An., 43, 509–539, 2003.

Gilbert, R. O.: Statistical methods for environmental pollution monitoring, Van Nostrand Reinhold, New York, 315 pp., 1987.

Garrick, M., Cunnane, C., and Nash, J. E.: A criterion of efficiency for rainfall runoff models, J. Hydrol., 36, 375–381, 1978.

Hasselmann, K.: Multi-pattern fingerprint method for detection and attribution of climate change, Clim. Dynam., 13, 601–612, 1997.

Hamlet, A. F. and Lettenmaier, D. P.: Effects of 20th century warming and climate variability on flood risk in the western US, Water Resour. Res., 43, W06427, doi:10.1029/2006WR005099, 2007.

Hirsch, R. M. and Slack, J. R.: A nonparametric trend test for seasonal data with serial dependence, Water Resour. Res., 20, 727–732, 1984.

Karl, T. R., Kukla, G., Razuvayev, V. N., Changery, M. J., Quayle, R. J., Heim Jr, R. R., Easterling, D. R., and Fu, C. B.: Global warming: Evidence for asymmetric diurnal temperature change, Geophys. Res. Lett., 18, 2253–2256, 1991.

Karl, T. R., Philip, D. J., Richard, W. K., et al.: Asymmetric trends of daily maximum and minimum temperature, B. Am. Meteorol. Soc., 74, 1007–1023, 1993.

Kendall, M. G.: Rank Correlation Methods, Charles Griffin, London, 272 pp., 1975.

Li, L.-J., Zhang, L., Wang, H., Wang, J., Yang, J.-W., Jiang, D.-J., Li, J.-Y., and Qin, D.-Y.: Assessing the impact of climate variability and human activities on streamflow from the Wuding River basin in China, Hydrol. Process., 21, 3485–3491, 2007.

Liu, S., Mo, X., Li, H., Peng, G., and Robock, A.: The spatial variation of soil moisture in China: Geostatistical Characteristics, J. Meteorol. Soc. Jpn., 79(2B), 555–574, 2001.

Liu, S., Leslie, L. M., Speer, M., Bunker, R., and Morison, R.: Approaching realistic soil moisture status in the Goulburn River catchment of southeastern Australia before and after a bushfire with an improved meso-scale numerical weather prediction model, in: Proceedings for the XXIII General Assembly of the International Union of Geodesy and Geophysics, Sapporo, Japan, June 30–July 11, 2003, IAHS Publ., 282, 215–320, 2003.

Liu, S., Mo, X., Lin, Z., Xu, Y., Ji, J., Wen, G., and Richey, J.: Crop yield response to Climate Change in the Huang-Huai-Hai Plain of China, Agricultural Water Management, in press, 2008.

Lorup, J. K., Refsgaard, J. C., and Mazvimavi, D.: Assessing the effect of land use change on catchment runoff by combined use of statistical tests and hydrological modelling: case studies from Zimbabwe, J. Hydrol., 205, 147–163, 1998.

Ma, Q. L., Wauchope, R. D., Hook, J. E., Johnson, A. W., Truman, C. C., Dowler, C. C., Gascho, G. J., David, J. G.,Summer, H. R., and Chandler, L. D.: Influence of tractor wheel tracks and crusts/seals on runoff: observations and simulations with the RZWQM, Agr. Syst., 51(1), 77–100, 1998.

Mahmood, R. and Hubbard, K.: An Analysis of Simulated Long-Term Soil Moisture Data for Three Land Uses under Contrasting Hydroclimatic Conditions in the Northern Great Plains,

J. Hydrometeorol., 5, 160–179, 2004.
Mann, H. B.: Nonparametric tests against trend, Econometrica, 13, 245–259. 1945.
Mo, X. and Liu, S.: Simulating evapotranspiration and photosynthesis of winter wheat over the growing season, Agr. Forest Meteorol., 109, 203–222, 2001.
Mo, X. and Beven, K.: Multi-objective conditioning of a three-source canopy model for estimation of parameter sensitivity and prediction uncertainty, Agr. Forest Meteorol., 122, 39–46, 2004.
Mo, X., Liu, S., Lin, Z., Chen, D., and Zhao, W.: Simulating the Water Balance of the Wuding River Basin in the loess Plateau with a Distributed Eco-hydrological model, Acta Geographica Sinica, 59(3), 341–348, 2004a.
Mo, X., Liu, S., Lin, Z., and Zhao, W.: Simulating temporal and spatial variation of evapotranspiration over the Lushi Basin, J. Hydrol., 285(1–4), 125–142, 2004b.
Mo, X., Liu, S., Lin, Z., Xu, Y., Xiang, Y., and McVicar, T. R.: Prediction of crop yield, water consumption and water use efficiency with a SVAT-crop growth model using remotely sensed data on the North China Plain, EcolModel., 183, 310–322, 2005.
Mo, X., Pappenberger, F., Beven, K., Liu, S., de Roo, A., and Lin, Z.: Parameter conditioning and prediction uncertainties of the LISFLOOD-WB distributed hydrological model, Hydrolog. Sci. J., 51(1), 45–65, 2006a.
Mo, X., Guo, R., and Lin, Z.: Responses of Gross Primary Productivity and Water Balance Components in Wuding River Region, the Eastern Part of the Loess Plateau from 1981 to 2001, Climatic and Environmental Research, 11(4), 477–486, 2006b.
Monteith, J. L. and Unsworth, M. H.: Principals of Environmental Physics, Edward Arnold, London, 2nd edn., 304 pp., 1990.
Nie, S., Luo, Y., and Jiang, Z.: Trends and Scales of Observed Soil Moisture Variations in China, Adv. Atmos. Sci., 25(1), 43–58, 2008.
Ouarda, T. B. M. J., Girard, G. S., Cavadias, C., and Bobee, B.: Regional flood frequency estimation with canonical correlation analysis, J. Hydrol., 254(1–4), 157–173, 2001.
Qian, Y., Dong, X., Qian, Y., and Chen, R.: The analysis to the change characteristics of streamflow and sediment load, Yellow river, 21(8), 25–29, 1999 (in Chinese).
Riad, S., Mania, J., Bouchaou, L., and Najjar, Y.: Rainfall-runoff model usingan artificial neural network approach, Math. Comput. Model., 40(7–8), 839–846, 2004.
Robock, A., Vinnikov, K. Y., Srinivasan, G., Entin, J. K., Hollinger, S. E., Speranskaya, N. A., Liu, S., and Namkhai, A.: The Global Soil Moisture Data Bank, B. Am. Meteorol. Soc., 81(6),

1281–1299, 2000.
Robock, A., Mu, M., Vinnikov, K., Trofimova, I. V., and Adamenko, T. I.: Forty five years of observed soil moisture in the Ukraine: No summer desiccation (yet), Geophys. Res. Lett., 32, L03401, doi:10.1029/2004GL021914, 2005.
Robock, A. and Li, H.: Solar dimming and CO_2 effects on soil moisture trends, Geophys. Res. Lett., 33, L20708, doi:10.1029/2006GL027585, 2006.
Salmi, T. M., Maatta, A., Anttila, P., Anttila, P., Ruoho-Airola, T., and Amnell, T.: Detesting trends of annual values of atmospheric pollutants by the Mann-Kendall Test and Sen's slope estimates – The Excel template application MAKESENS, Finnish Meteorological Institute, Helsinki, 2002.
Sauquet, E. and Leblois, E.: Discharge analysis and runoff mapping applied to the evaluation of model performance, Phys. Chem. Earth Pt. B, 26(5/6), 473–478, 2001.
Schlosser, C. A., Slater, A. G., Robock, A., Pitman, A. J., Vinnikov, K., Henderson-Sellers, A., Speranskaya, N. A., Mitchell, K., and the PILPS 2(d) Contributors: Simulations of a boreal grassland hydrology at Valdai, Russia: PILPS Phase 2(d), Mon. Weather Rev., 128, 301–321, 2000.
Sheffield, J. and Wood, E.: Global Trends and Variability in Soil Moisture and Drought Characteristics, 1950–2000,from Observation-Driven Simulations of the Terrestrial Hydrologic Cycle, J. Climate, 21, 432–458, 2008.
Shuttleworth, W. J. and Wallace, J. S.: Evaporation from sparse crops – an energy combination theory, Q. J. Roy. Meteor. Soc., 111, 839–855, 1985.
Stenchikov, G. L. and Robock, A.: Diurnal asymmetry of climatic response to increased CO_2 and aerosols: Forcings and feedbacks, J. Geophys. Res., 100, 26 211–26 227, 1995.
Tao, F., Yokozawa, M., Hayashi, Y., and Lin, E.: Future climate change, the agricultural water cycle, and agricultural production in China Agriculture, Ecosystems and Environment, 95(1), 203–215, 2003.
Wagner, W., Lemoine, G., and Rott, H.: A Method for Estimating Soil Moisture from ERS Scatterometer and Soil Data, Remote Sens. Environ., 70(2), 191–207, 1999.
Weglarczyk, S.: The interdependence and applicability of some statistical quality measures for hydrological models, J. Hydrol., 206, 98–103, 1998.
Xu, J., Wang, L., Xu, S., and Qiao, Y.: Analys is of Dam-Break and Flood in Shaanxi Northern Region, Northwest Water Resources and Water Engineering, 11(4), 88–91, 2000 (in Chinese).

Xu, J.: Response of erosion and sediment producing processes to soil and water conservation measures in the Wuding River Basin, Acta Geographica Sinica, 59(6), 972–981, 2004 (in Chinese).

Yan, J., Wang, X., Sun, H., and Chen, L.: On Progressive Decrease Rate of Surface Runoff at Different Periods in Arid Regions of Shaanxi and Gansu Provinces, Scientia Geographica Sinica, 19(6), 532–535, 1999.

Yang, X., Yan, J., and Liu, B.: The analysis on the change characterisitics and driving forces and driving forces of WudingRiver runoff, Advances in Earth Sciences, 20(6), 637–642, 2005 (in Chinese).

Yin, Z., Shao, X., Qin, N., and Liang, E.: Reconstruction of a 1436-year soil moisture and vegetation water use history based on tree-ring widths from Qilian junipers in northeastern Qaidam Basin, Northwestern China, Int. J. Climatol., 28, 37–53, 2008.

Zhang, S. L., Li, Z., and Zhao, W. L.: Changes in Streamflow and Sediment Load in the Coarse Sandy Hilly Areas of the Yellow River Basin, The Yellow River Water Conservancy Press,191 pp., 1998 (in Chinese).

Zhang, X., Zwiers, F. W., Hegerl, G. C., Lambert F. H., Gillett, N. P., Solomon, S., Stott, P. A., and Nozawa, T.: Detection of human influence on twentieth-century precipitation trends, Nature, 448(26), 461–465, doi:10.1038/nature06025, 2007.

Zhao, X. and Yan, X.: The Trend of soil moisture storage in the last 20 years and its countermeasures of water management and regulation over north China, Climatic and Environmental Research, 11(3), 371–379, 2006 (in Chinese).

Table 1. The mean, range (=max−min) and the maximum of C_v for the 11 variables at the daily, monthly and annual scale.

	R_n	E_T	E_C	E_S	E_I	L_{AI}	θ_1	θ_2	P	T	Q
						Daily					
mean	1.08	0.31	0.40	0.35	1.89	0.20	0.26	0.18	2.93	0.81	0.65
range	20.02	0.24	1.24	0.41	6.28	1.84	0.24	0.12	4.75	45.80	2.78
max	20.19	0.43	1.43	0.62	6.86	1.84	0.43	0.26	6.15	45.88	2.97
						Monthly					
mean	0.49	0.20	0.26	0.23	0.50	0.18	0.20	0.17	0.75	0.24	0.13
range	4.21	0.15	0.60	0.21	0.66	0.82	0.08	0.05	0.82	0.75	0.49
max	4.27	0.30	0.77	0.33	0.87	0.82	0.24	0.20	1.20	0.78	0.50
						Annualy					
mean	0.82	0.92	1.33	0.70	2.31	1.53	0.28	0.17	3.14	1.17	1.06
range	0.15	0.24	0.24	0.34	0.91	0.28	0.19	0.17	1.75	0.51	2.18
max	0.87	1.07	1.46	0.88	2.82	1.65	0.36	0.27	4.21	1.47	2.68

Note: For R_n, not include the four large vaues (41.47, 381.43, 131.1, 456.92) when doing the calculation.

HESSD
5, 3557–3604, 2008

Table 2. The decade mean of SM (the first line) and the ratio of the difference between the decade mean and the multi-year average to the multi-year average (the second line) for precipitation (P), net radiation (R_n), evapotranspiration (E_T), GPP, NPP, runoff (Q), root zone SM (θ_2) and air temperature (T) of the Wuding River basin.

	P	R_n	E_T	E_C	E_S	EI	GPP	NPP	Q	θ_2	T
1950s	502.3	776.4	442.3	237.2	193.3	11.9	42.2	243.0	103.7	0.12	9.73
	0.16	0.00	0.09	0.10	0.07	0.05	0.04	0.18	0.72	0.05	−0.03
1960s	482.8	785.9	421.5	216.2	194.2	11.1	37.2	188.1	93.7	0.1	9.73
	0.11	0.01	0.03	0.00	0.08	−0.02	−0.09	−0.08	0.56	0.12	−0.03
1970s	422.9	773.7	402.8	213.1	178.1	11.6	38.9	199.5	55.8	0.1	9.83
	−0.02	0.00	−0.01	−0.01	−0.01	0.03	−0.05	−0.03	−0.07	0.03	−0.02
1980s	418.5	762.7	403.9	216.0	176.7	11.2	42.3	213.4	49.5	0.1	9.80
	−0.03	−0.02	−0.01	0.00	−0.02	−0.01	0.04	0.04	−0.18	−0.03	−0.02
1990s	392.9	777.4	391.8	212.7	168.1	11.0	43.1	209.0	36.2	0.1	10.6
	−0.09	0.00	−0.04	−0.02	−0.07	−0.03	0.06	0.02	−0.40	−0.11	0.05
2000s	424.9	777.5	408.1	217.4	179.1	11.6	42.6	203.4	45.1	0.1	10.74
	−0.02	0.00	0.00	0.01	−0.01	0.03	0.05	−0.01	−0.25	−0.02	0.07

HESSD
5, 3557–3604, 2008

Table 3. The statistics of Mann-Kendall trend and Sen's slope estimate for the eight variables. Z, μ, B are explained in Sect. 2.2. μ_{min99} expreses the lower limit of the 99% confidence interval of μ (α=0.01). μ_{max95} expreses the upper limit of the 95% confidence interval of μ (α=0.05). The definition of the upper and lower limit is shown in Sect. 2.2.

Variable	Test Z	Signi-ficance	μ	μ_{min99}	μ_{max99}	μ_{min95}	μ_{max95}	B	B_{min99}	B_{max99}	B_{min95}	B_{max95}
P	−1.72	+	−1.90	−4.52	0.89	−3.93	0.28	474.6	533.7	415.9	518.7	428.6
R_n	−1.03		−0.27	−1.05	0.44	−0.81	0.27	782.5	794.7	766.2	791.6	769.0
ET	−1.54		−0.73	−2.08	0.52	−1.81	0.19	427.3	452.5	399.6	447.8	408.6
EC	−0.42		−0.18	−0.92	0.70	−0.70	0.49	225.3	241.0	201.8	238.7	208.5
ES	−2.07	*	−0.56	−1.18	0.19	−0.99	−0.05	191.3	207.8	174.5	202.5	181.8
EI	−0.35		−0.01	−0.06	0.06	−0.05	0.04	11.7	13.0	9.8	12.6	10.2
GPP	3.10	**	0.15	0.03	0.27	0.06	0.23	38.1	40.5	34.5	39.7	36.0
NPP	0.65		0.30	−0.69	1.19	−0.44	0.98	201.8	227.8	174.8	218.9	179.8
Q	−3.33	***	−0.85	−1.73	−0.16	−1.45	−0.35	69.5	93.1	52.9	86.7	57.6
θ_2	−2.83	**	−0.001	−0.001	−0.00	−0.001	−0.00	0.13	0.15	0.12	0.14	0.12
T	3.39	***	0.023	0.006	0.041	0.010	0.037	9.4	9.8	9.1	9.8	9.2

*** if trend at α=0.001 level of significance; ** if trend at α=0.01 level of significance; * if trend at α0.05 level of significance; + if trend at α0.1 level of significance.

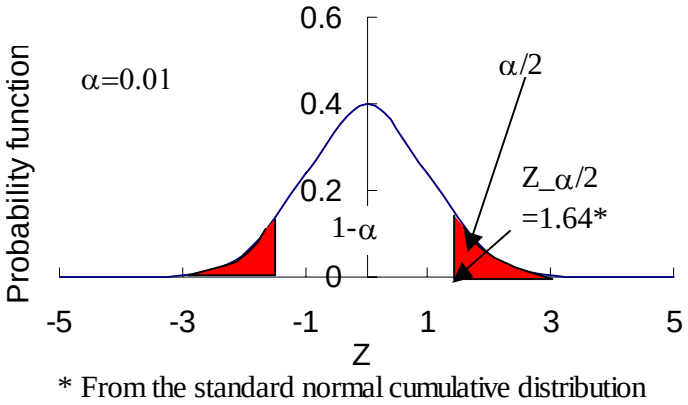

Fig. 1. The normal distribution for the two-tailed hypothesis test in Mann-Kendall method.

HESSD
5, 3557–3604, 2008

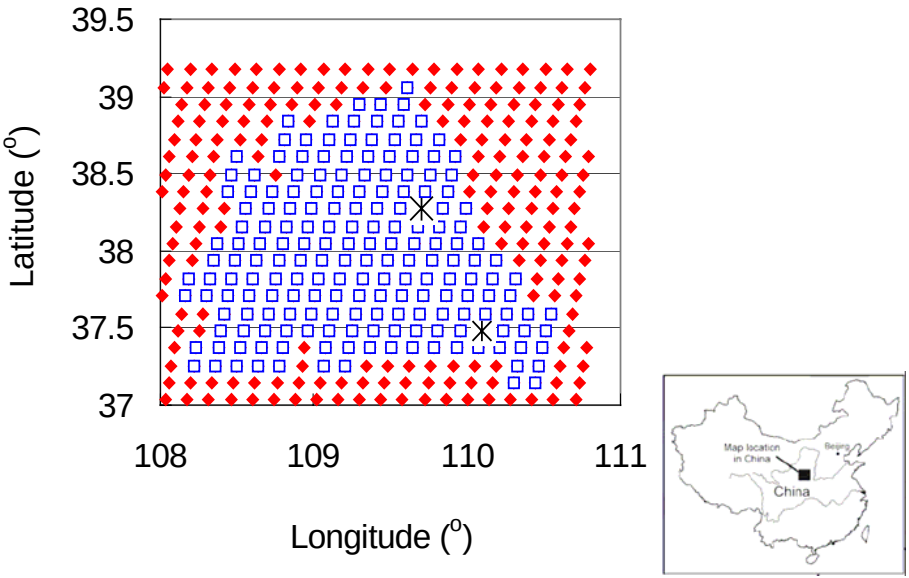

Fig. 2. The SM data distribution (Red dots: TUW grid point (12.5×12.5 km) of the ERS scatterometer-derived SM data; 189 blue square: VIP grid point (8×8 km, matched with TUW grid) of SM (Relative water content of soil surface (2.5 cm, wc/wcsat) simulated by VIP model. Black star: Observed point of SM – relative water content of soil surface (10 cm, wc/wcsat) observed at Suide and Yulin.

HESSD
5, 3557–3604, 2008

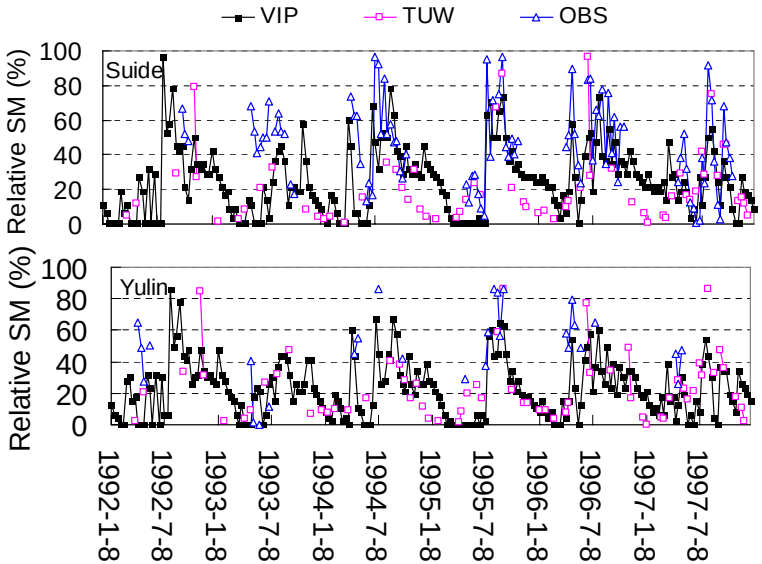

Fig. 3. The yearly evolution of relative SM simulated by VIP, retrieved from remote sensing TUW data and observation at Suide and Yulin.

HESSD
5, 3557–3604, 2008

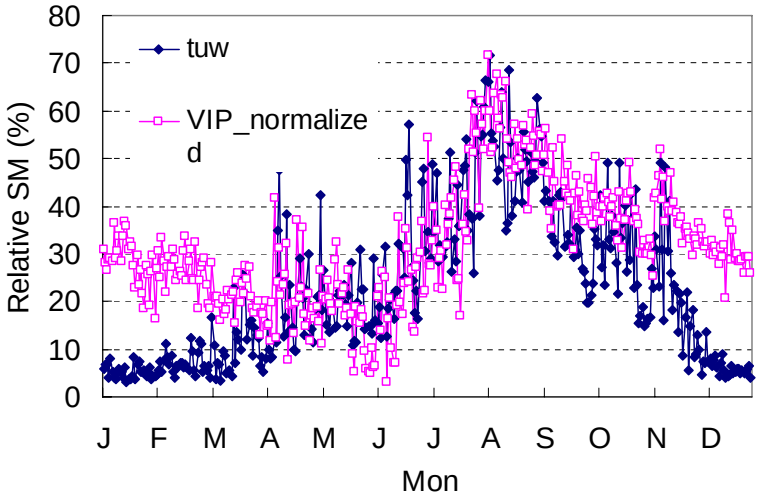

Fig. 4. The averaged **(a)** seasonal variation and **(b)** yearly evolution of relative SM over the 189 grid points simulated by VIP and retrieved from remote sensing by TUW.

HESSD
5, 3557–3604, 2008

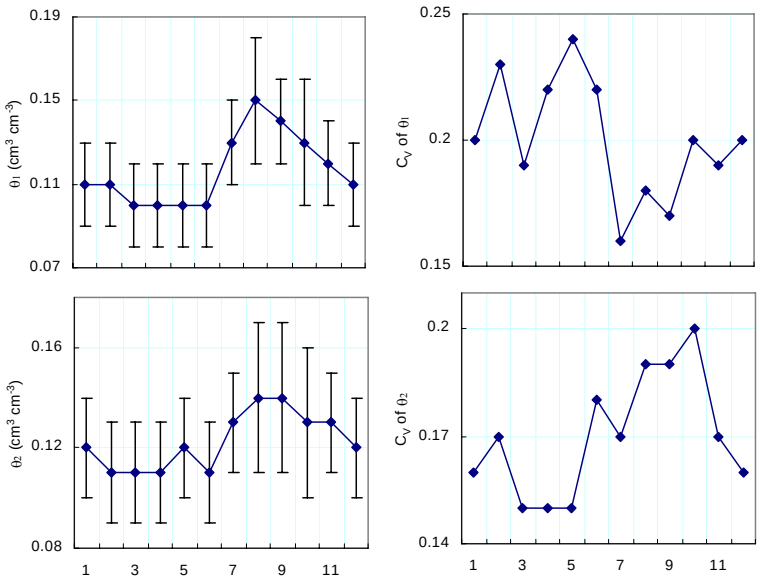

Fig. 5. Average seasonal cycle of monthly mean SM in the 0–2 cm surface layer (θ_1) and root zone (θ_2) (left panel) and their variability (right panel) averaged over the entire data records (1957–2004). Months are indicated with the numbers on the abscissa. Shown in the figure is also the one standard deviation.

HESSD
5, 3557–3604, 2008

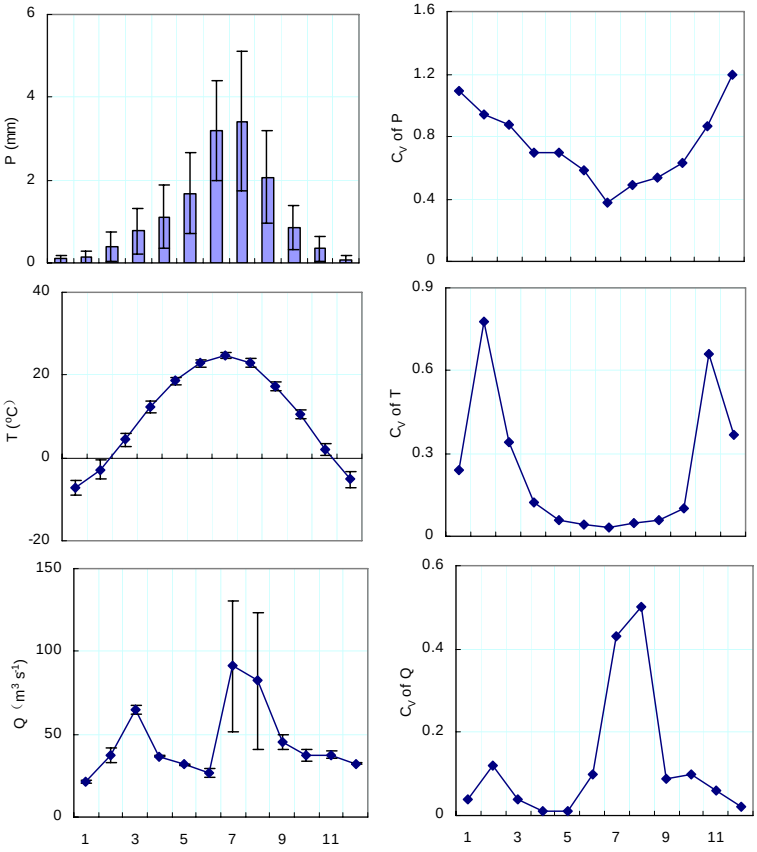

Fig. 6. Average seasonal cycle of precipitation (P), air temperature (T) and runoff (Q) at the control station of the basin (represented by the mean value over each month, left panel)and their variability (right panel) averaged over the entire data records (1957–2004). Months are indicated with the numbers on the abscissa. Shown in the figure is also the one standard deviation.

HESSD
5, 3557–3604, 2008

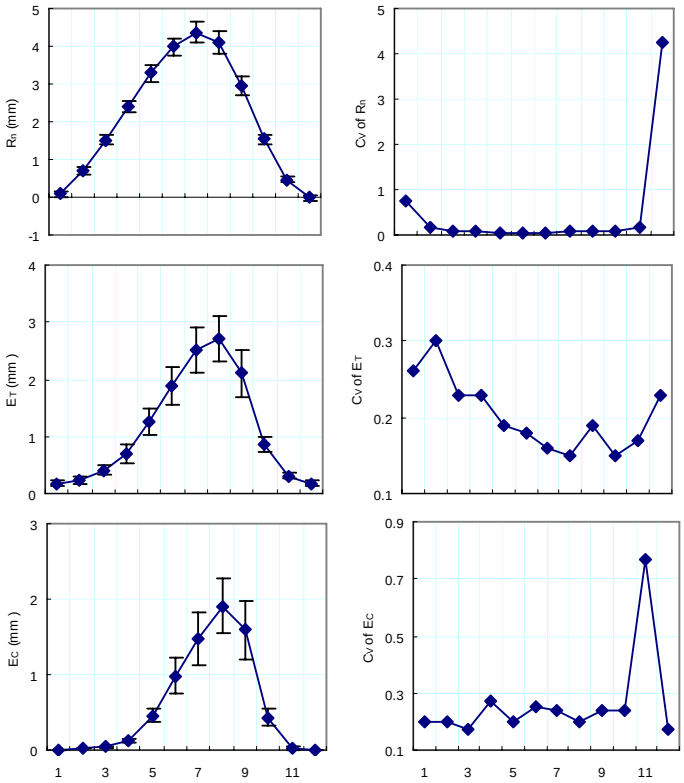

Fig. 7a. Average seasonal cycle of net radiation (R_n), total evapotranspiration (E_T), canopy transpiration (E_C), soil evaporation (E_S), evaporation form the intercepted precipitation by the canopy (E_I) and Leaf area index (L_{AI})(represented by the mean value over each month, left panel) and their variability (right panel) averaged over the entire data records (1957–2004). Months are indicated with the numbers on the abscissa. Shown in the figure is also the one standard deviation.

HESSD
5, 3557–3604, 2008

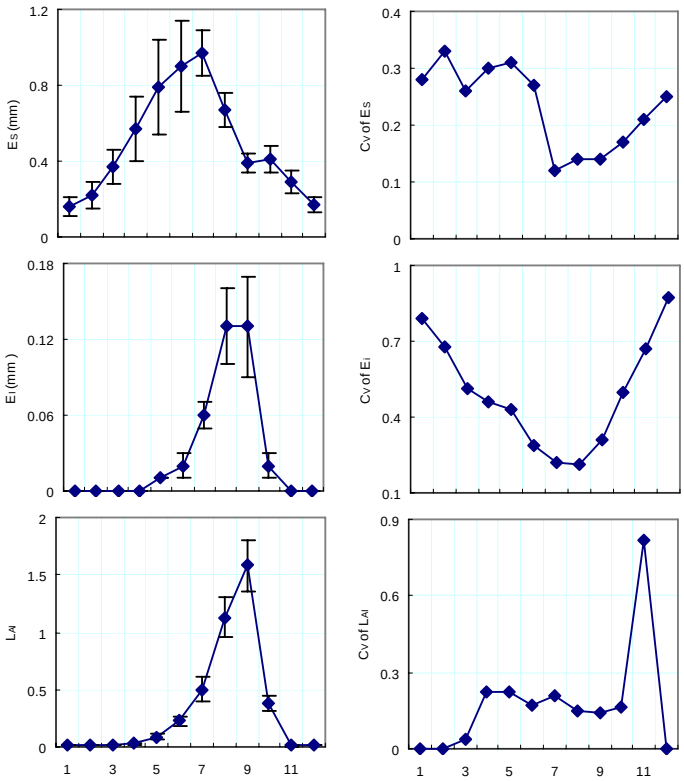

Fig. 7b. Same as Fig. 7a, but for soil evaporation (E_S), evaporation form the intercepted precipitation by the canopy (E_I) and Leaf area index (L_{AI}).

HESSD

5, 3557–3604, 2008

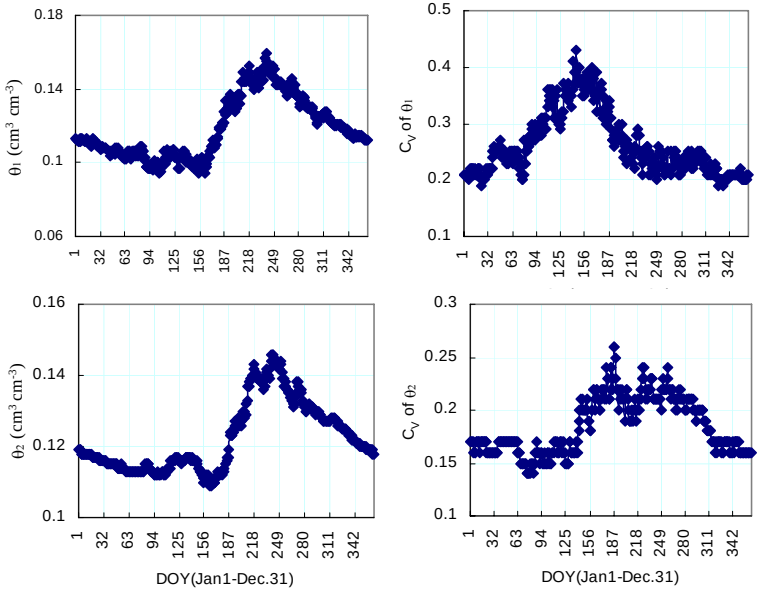

Fig. 8. Mean daily SM (left panel) and SM variability (right panel) at daily time scale in the 0–2 cm surface layer (θ_1) and root zone (θ_2). Day 1=1 January.

HESSD
5, 3557–3604, 2008

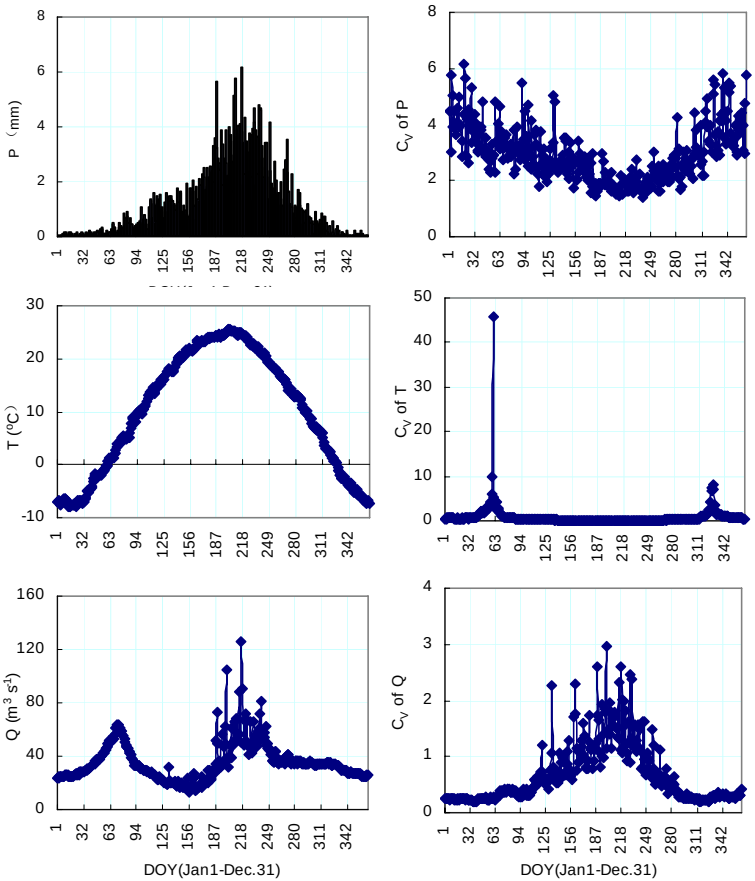

Fig. 9. Mean daily values (left panel) and their variability (right panel) at daily time scale for precipitation (P), air temperature (T) and runoff (Q) at the control station of the basin. Day 1=1 January.

HESSD
5, 3557–3604, 2008

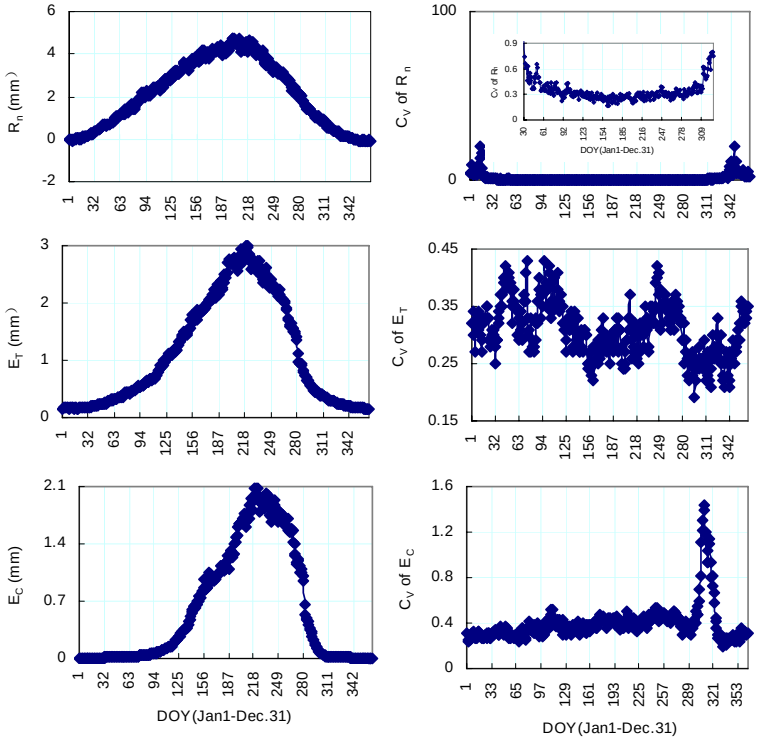

Fig. 10a. Mean daily values (left panel) and their variability (right panel) at daily time scale for net radiation (R_n), total evapotranspiration (E_T), canopy transpiration (E_C). Day 1=1 January.

HESSD

5, 3557–3604, 2008

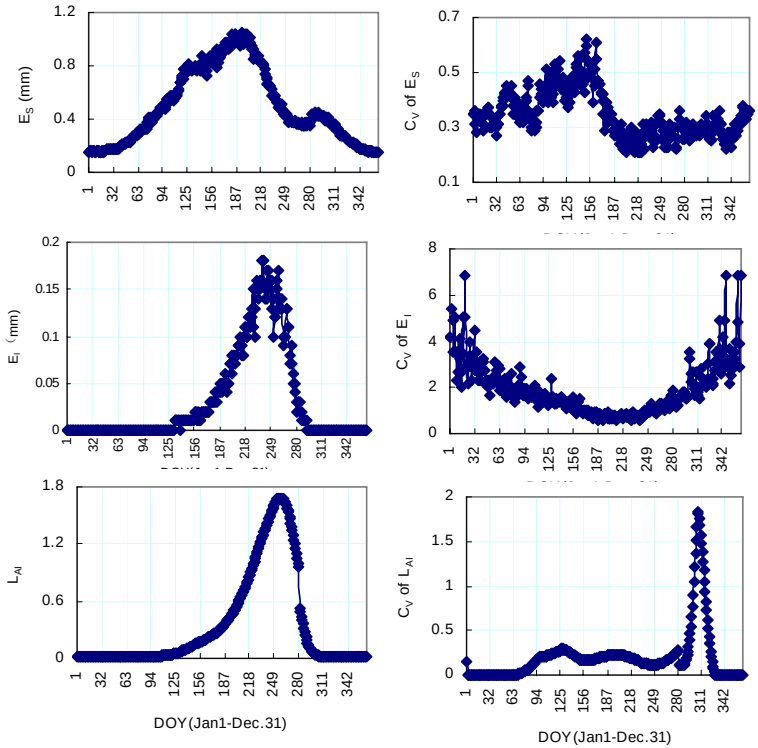

Fig. 10b. Same as Fig. 10a but for soil evaporation (E_S), evaporation from the intecepted precipitation by the canopy (E_I) and Leaf area index (L_{AI}).

HESSD
5, 3557–3604, 2008

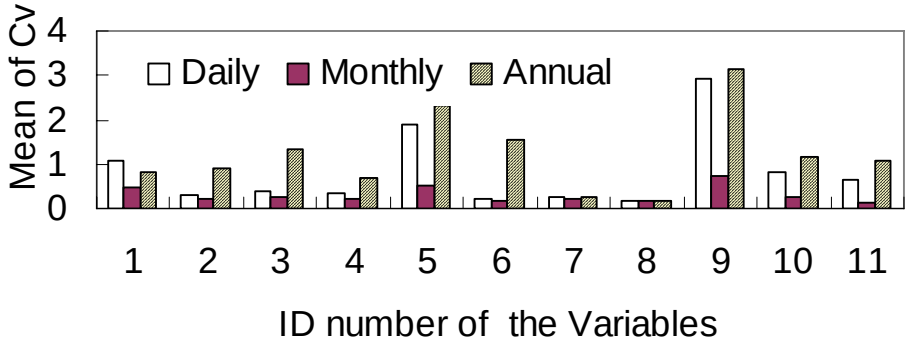

Fig. 11. The mean of the C_V at the daily, monthly and annual scale (the ID number in the abscissa 1~11 represents R_n, E_T, E_C, E_S, E_I, L_{AI}, θ_1, θ_2, P, T, and Q). For R_n, the four large values (41.47, 381.43, 131.1, 456.92) are not included.

HESSD
5, 3557–3604, 2008

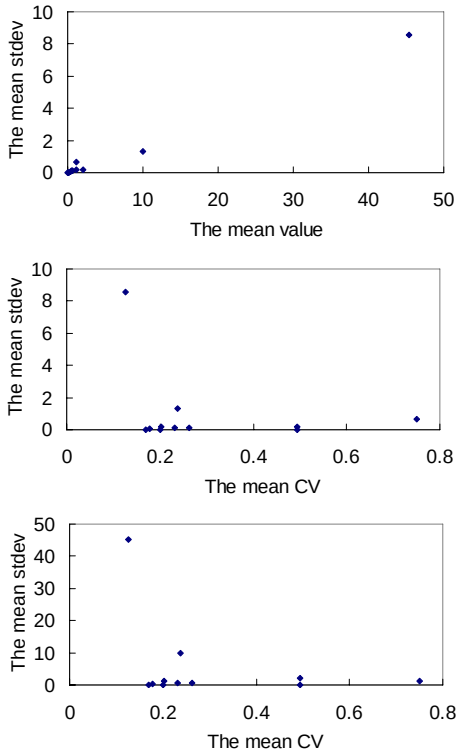

Fig. 12. The comparison among the value, standard deviation and the coefficient of variation for the 11 variables.

HESSD
5, 3557–3604, 2008

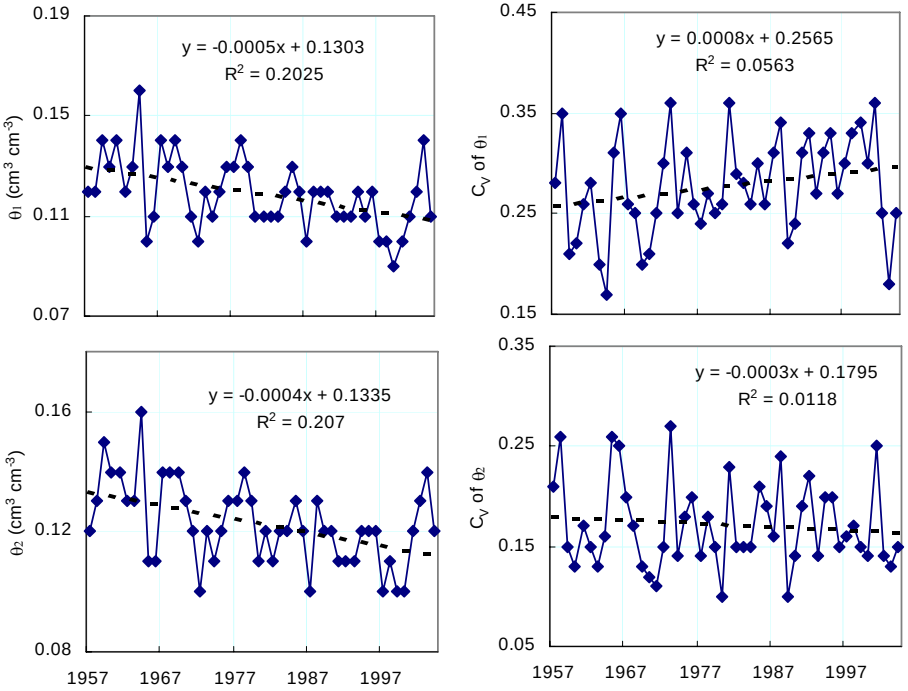

Fig. 13. The annual mean of SM in the 0–2 cm surface layer (θ_1) and root zone (θ_2) (left panel) and their variability (right panel) over the years.

HESSD

5, 3557–3604, 2008

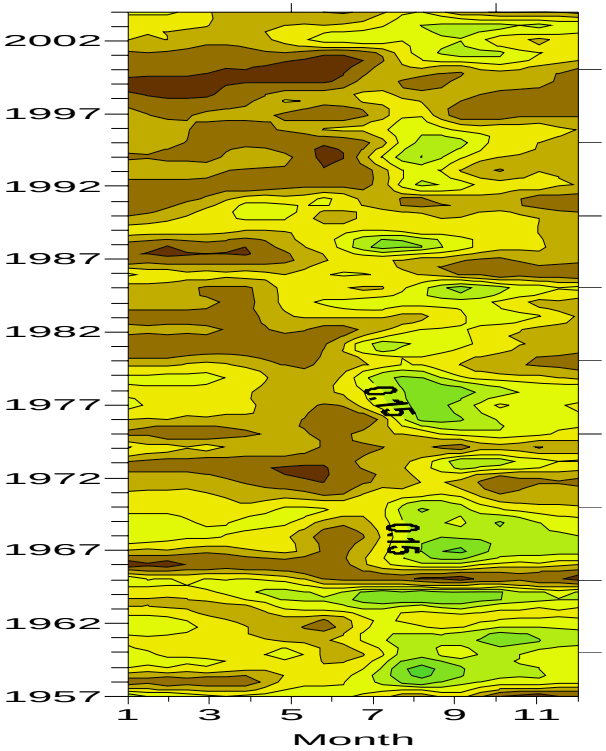

Fig. 14. Year/month plot of SM variations in the root zone, averaged over the Wuding River basin.

HESSD

5, 3557–3604, 2008

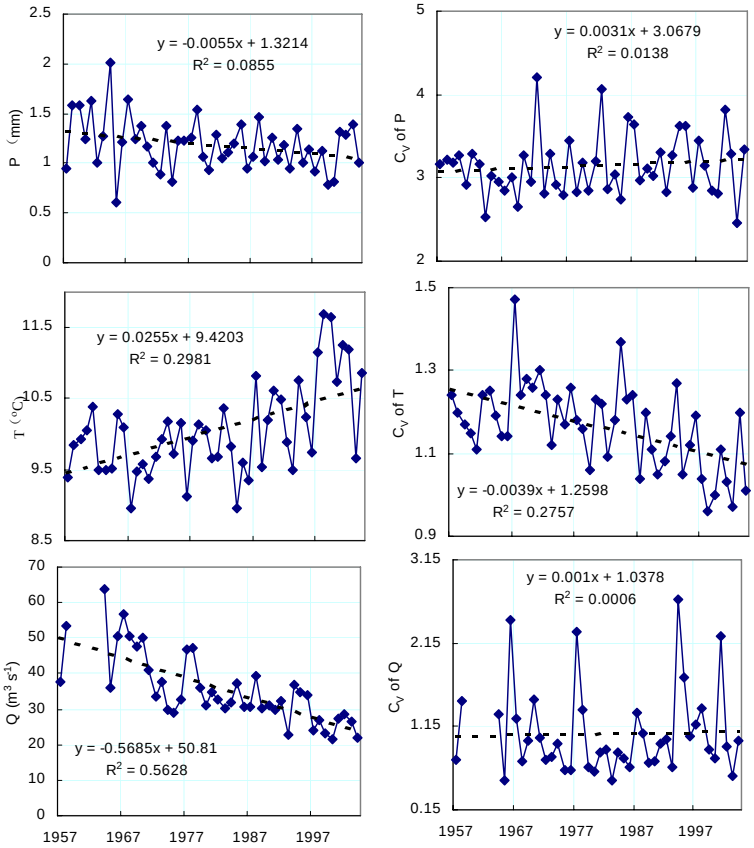

Fig. 15. The annual mean of precipitation (P), air temperature (T) and runoff (Q) at the control station of the basin (left panel) and their variability (right panel) over the years.

HESSD
5, 3557–3604, 2008

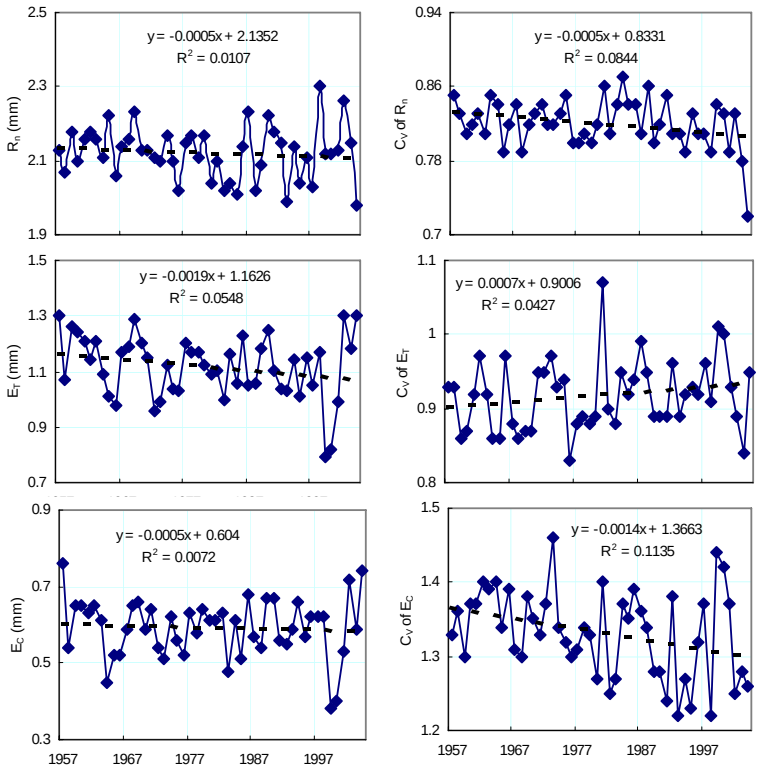

Fig. 16a. The annual mean of net radiation (R_n), total evapotranspiration (E_T), canopy transpiration (E_C) (left panel) and their variability (right panel) over the years.

HESSD
5, 3557–3604, 2008

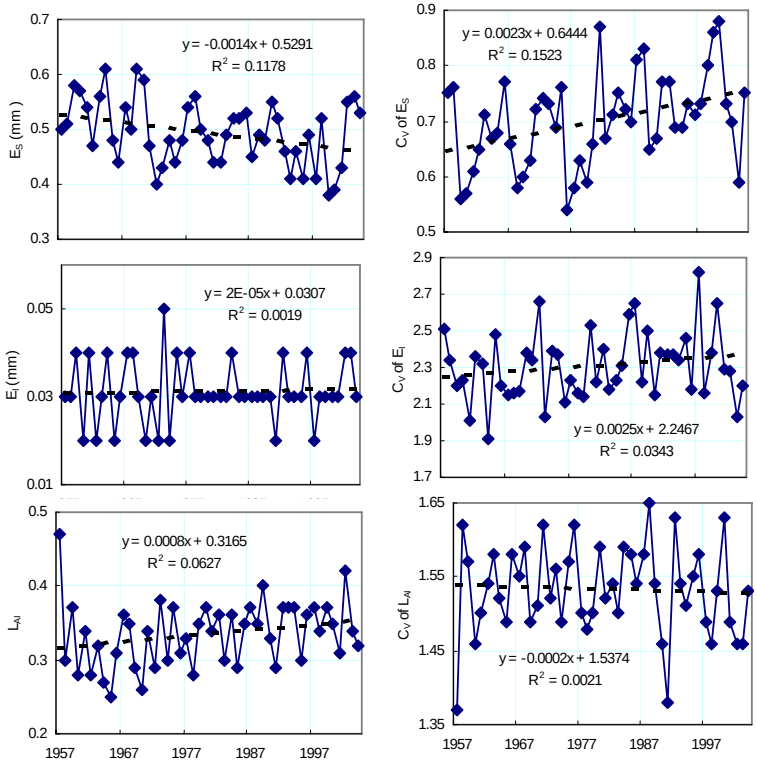

Fig. 16b. The same as Fig. 16a but for soil evaporation (E_S), evaporation form the intercepted precipitation by the canopy (E_I) and Leaf Area Index (L_{AI}).

HESSD
5, 3557–3604, 2008